Optics Letters

Microfabricated strontium atomic vapor cells

Jacob M. Pate,[1,2] John Kitching,[2] and Matthew T. Hummon[2,*]

[1]Department of Physics, University of Colorado Boulder, Boulder, Colorado 80309, USA
[2]National Institute of Standards and Technology, Boulder, Colorado 80305, USA
*Corresponding author: matthew.hummon@nist.gov

Received 26 September 2022; revised 27 October 2022; accepted 18 November 2022; posted 9 December 2022; published 5 January 2023

We demonstrate strontium (Sr) atomic vapor cells having a total external volume of 0.63 cm^3 that can operate above 300 °C for times exceeding 380 h. The cells are fabricated using micromachined silicon frames anodically bonded to glass windows that have a 20-nm thick protective layer of Al_2O_3 deposited on the interior surfaces. The presence of Sr vapor in the cell is confirmed through laser absorption spectroscopy for the $^1S_0 \rightarrow {}^1P_1$ transition in Sr at 461 nm. Measurements of sub-Doppler linewidths indicated negligible (<3 MHz) broadening of this transition from residual background gas collisions. This compact and manufacturable, high-temperature atomic vapor cell can enable narrow-line optical frequency references based on strontium and other alkaline earth species.

https://doi.org/10.1364/OL.476552

Warm atomic vapors enable a wide range of devices for sensing and metrology by providing a robust, simple platform for precision measurement of a quantum system. For example, Rydberg states in alkali atoms can couple strongly to microwave electric fields, and techniques for detecting microwave fields in both magnitude and phase have been demonstrated [1–3]. Atomic magnetometers based on the interrogation of atomic spin orientation have also been used in a wide range of applications, such as magnetoencephalographic measurements of the human brain [4], gyroscopes for navigation [5,6], mapping subterranean features [7,8], and identifying explosive devices [9]. Precision microwave spectroscopy of ground state alkali atomic vapors provides the basis for compact atomic clocks [10], and the development of compact optical frequency references using warm atomic and molecular vapors shows a path toward the next generation of compact, high-performance optical timing [11,12]. Properties of alkaline earth atoms, such as the existence of narrow linewidth intercombination transitions and bosonic isotopes with zero nuclear spin [13], can offer advantages for certain applications, such as optical frequency references [14] and primary Doppler thermometry at high temperatures [15]. Development of robust fabrication techniques for alkaline earth atomic vapor cells, therefore, promises to expand the field of compact quantum sensing.

One of the main challenges faced in the design of alkaline earth vapor cells is the high operating temperature required for generating sufficient vapor pressure for spectroscopy, typically ranging from 300 °C to 500 °C [16,17]. At these elevated temperatures, the alkaline earth vapor attacks standard borosilicate and fused silica windows and renders them opaque [18,19]. Traditional approaches to incorporate alkaline earth atoms for spectroscopy include heat pipes [17,20,21], cells with solid crystalline windows (sapphire, CaF_2, CaF_2:Eu) [18–20,22], hollow-cathode lamps [23], and atomic beams [24,25]. Heat pipes can avoid the need for glass protection through the generation of cold spots, but occupy a much larger volume. Cells with crystalline windows in small packages provide robust protection from the alkaline earth vapor, but the high temperatures required for hermetic sealing methods, such as glass transfer tape (800°C) [19] or diffusion bonding (1400°C) [26], make it challenging to incorporate them into widely adopted silicon fabrication technologies. Low-temperature indium seals for CaF_2:Eu have been tested with limited success [18], while optical contacting of CaF_2:Eu has shown some promise [16]. Alternative approaches to high-temperature operation, such as laser-controlled vapor production from an alkaline earth oxide [27,28], produce enough atoms to load a magneto-optical trap, though further investigation is necessary for their use in vapor cell applications. Previous work investigating thin film Al_2O_3 coatings in alkali atom vapor cells [29,30] indicates an increase in vapor cell operation lifetime for temperatures up to 300 °C.

In this Letter, we report the development of a microfabricated strontium atomic vapor cell compatible with standard silicon fabrication techniques. We incorporate Al_2O_3 protection of the cell windows using atomic layer deposition onto glass substrates to extend the operational lifetime. We characterize the vapor cell performance at temperatures greater than 300 °C by performing spectroscopy measurements on the strontium $^1S_0 \rightarrow {}^1P_1$ transition at $\lambda = 461$ nm and validate the presence of Sr vapor and low background gas contamination within the vapor cells. Operation of these microfabricated alkaline earth atomic vapor cells in excess of 380 h demonstrates their potential for enabling a new class of compact, low-power quantum sensors.

Figure 1(a) shows a completed microfabricated strontium vapor cell. Two chambers are formed in a 3-mm thick silicon wafer using deep reactive ion etching (DRIE). A reservoir chamber (3 mm × 5 mm) houses the strontium metal and is connected to the optical probe chamber (6 mm × 5 mm) through baffles angled at 45°. The baffles are created to prevent line-of-sight access between the two chambers and avoid the generation of an atomic beam, but rather create a vapor. The glass windows used to seal the vapor cell are coated on one side with a 20-nm thin layer of Al_2O_3 through commercial atomic layer deposition (ALD). In previous work on alkali metal vapor cells [29], a

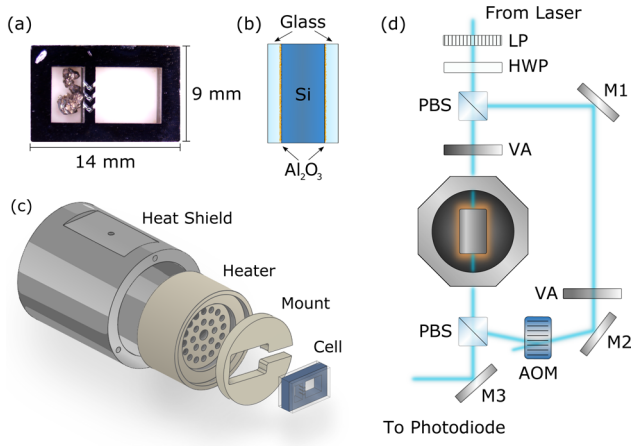

Fig. 1. (a) Fully assembled vapor cell after anodic bonding with granular pieces of strontium in the reservoir chamber. (b) Side view of cell (not to scale), highlighting composite layers and aluminum oxide deposition. (c) Oven schematic and layout. Nickel chromium wire is woven through the holes in the boron nitride. A 3-mm diameter hole along the cylinder axis provides optical access to the probe chamber of the cell. (d) Optical measurement for absorption (pump blocked) and saturated absorption measurements. Polarizing beam splitters (PBSs), linear polarizer (LP), a half-wave plate (HWP), variable attenuators (VAs), an acousto-optic modulator (AOM), and mirrors (M1, M2, M3) are shown for clarity.

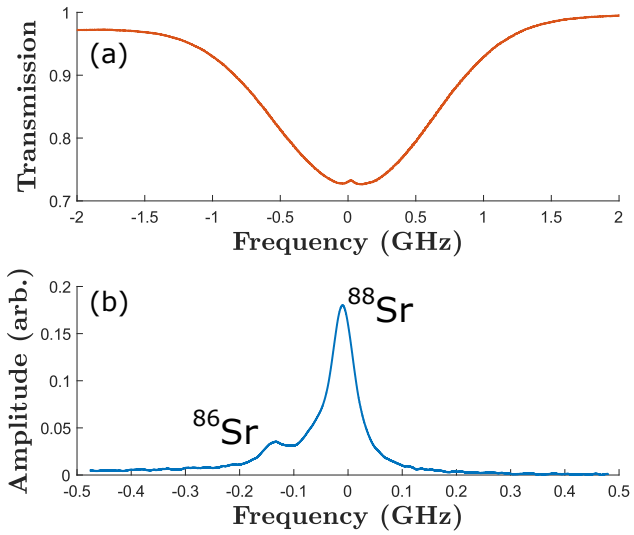

Fig. 2. (a) Normalized strontium absorption through cell without averaging. (b) Sub-Doppler peaks are shown clearly as a result of the AOM chopper configuration. The smaller peak is representative of ^{86}Sr and is used to calibrate the frequency axis.

20-nm thick layer shows sufficient protection, while still being thin enough for anodic bonding to proceed [31]. After the first window is anodically bonded to the silicon frame, the strontium metal (99.99 % purity) is loaded into the reservoir chamber under an argon atmosphere, quickly transferred in air to the wafer bonder, and the wafer bonding chamber is evacuated to a pressure below 7.5×10^{-5} Torr (1×10^{-4} hPa). The transfer process usually takes less than 1 min to ensure a clean sample of strontium. The cell is completed by anodically bonding the final top window in the evacuated bonding chamber at 300 °C to 400 °C with 1 kV applied across the silicon and glass. Figure 1(b) shows the layers of a completed vapor cell. Throughout this Letter, the terms "coated" and "uncoated" refer specifically to any glass with or without a 20-nm layer of Al_2O_3, respectively.

Strontium has a much lower vapor pressure than, for example, alkali atoms, and therefore requires substantially elevated temperatures to achieve significant optical absorption. The cells were therefore placed inside an oven contained in an evacuated enclosure to elevate the cell temperature to a point where the strontium vapor density resulted in 50 % absorption [Fig. 1(c)]. The custom-built oven (within the vacuum chamber) consists of a stainless-steel heat shield (4 cm long and 3.5 cm in diameter) and houses the electrically insulating, thermally conductive boron nitride core that was machined to thread 36-gauge nickel chromium wire with a number of passes to provide resistive heating. An opening on the side of the vapor cell mount allows a thermocouple to be placed near the cell to estimate the oven temperature. The thermally conductive thermocouple may create a cold spot at the side of the cell, which could prevent condensation of Sr on the windows during thermal cycling, although no attempt was made to characterize this effect.

Doppler-free spectroscopy was carried out at $\lambda = 461$ nm using a counterpropagating pump–probe configuration, as shown in Fig. 1(d). An AOM allows amplitude modulation of the pump beam, enabling removal of the Doppler-broadened background through lock-in detection. Figure 2(a) shows a typical absorption spectrum taken using the microfabricated vapor cell at an oven operating temperature around 320 °C. It consists of a wide Doppler-broadened feature with absorption of the order of 25 %, and a smaller sub-Doppler resonance near zero detuning, generated from the counterpropagating pump beam. This curve depicts the main absorption with no averaging and is representative of typical data. Assuming a 3-mm long absorption path length, from the 25 % Doppler-broadened absorption we estimate a Sr density of 4×10^{10} cm^{-3}, corresponding to an equilibrium vapor pressure temperature of 325 °C [32], consistent with the estimated oven temperature. The Doppler linewidth measured from fitting the data to a Voigt profile is about 30 % larger than would be expected from an estimate from the oven thermocouple temperature, though the disparity in the measurements may be due to imprecise estimates of Sr vapor pressure and thermal gradients between the thermocouple and atomic vapor.

Figure 2(b) shows the sub-Doppler spectrum, where the broad Doppler profile has been eliminated via lock-in detection of the probe beam at the pump beam amplitude modulation frequency. This technique allows for clear identification of the sub-Doppler absorption peaks of the two most abundant isotopes, ^{86}Sr and ^{88}Sr. To calibrate the frequency axis of our spectra, we use the known detuning of the ^{86}Sr transition from the main ^{88}Sr line, $\Delta = -124.5$MHz [23]. In a second calibration method, a strong RF modulation of the laser frequency, of $\Omega_{\mathrm{mod}} = 120$ MHz, is applied to the pump and probe beams. This imprints peaks on the sub-Doppler spectroscopy signal, with spacing equal to $\Omega_{\mathrm{mod}}/2$. The spectroscopy signal is fit to a sum of Lorentzian profiles with a frequency-scaling factor to obtain the correct 60-MHz separation. A comparison of these two methods yields a frequency calibration uncertainty of 1.2 %.

Figure 3 shows a measurement of the sub-Doppler feature linewidth as a function of total pump and probe power. The data are fit to a power-broadening function of the form $\Gamma =$

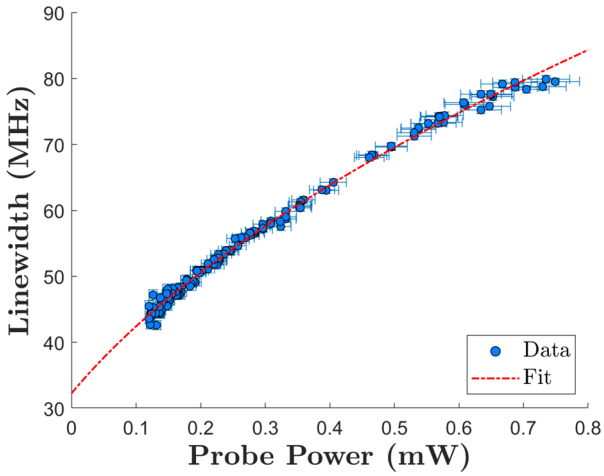

Fig. 3. Sub-Doppler linewidth measurements as a function of total probe power. The zero-power intercept yields a linewidth $\Gamma_0/2\pi = 32.3 \pm 0.5 \pm 0.4$ MHz, which accounts for uncertainties in Lorentzian fitting and frequency calibration. Error bars represent a 68 % confidence interval.

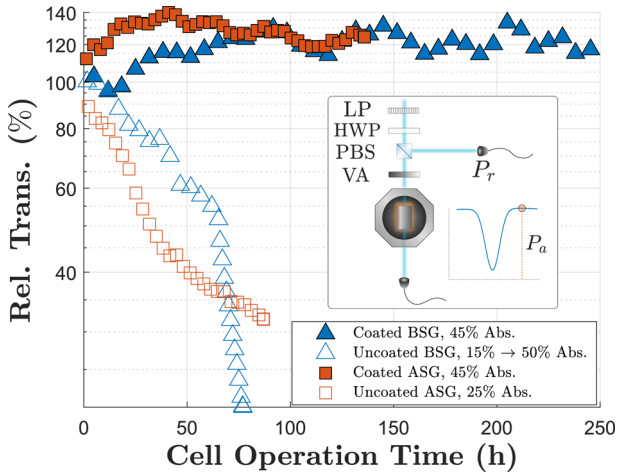

Fig. 4. Comparison of operational lifetime measurements for vapor cells with and without 20-nm thick Al_2O_3 window coatings. Filled markers correspond to cells with sapphire coating and empty markers represent standard glass. The coating is shown to extend the lifetime of the cell for both aluminosilicate glass (ASG) and borosilicate glass (BSG) substrates. The inset shows the experimental setup to monitor the relative transmission through the vapor cell. We measure both the off resonance transmission through the cell, P_a, and a reference beam power, P_r, measured before the vapor cell for normalization of the relative transmission.

$\Gamma_0\,(1 + P/P_s)^{1/2}$, where Γ_0 is the natural linewidth and P_s is the saturation power for the transition. From the fit, we infer a zero-power linewidth of $\Gamma_0/2\pi = 32.3 \pm 0.5 \pm 0.4$ MHz, representing 68 % confidence intervals for linewidth fitting and frequency scaling, respectively. Recent measurements using photoassociative spectroscopy [33–35] yield a transition linewidth of $2\pi\times30.2$ MHz. Comparing these two sets of measurements results in an upper limit of 2.7 MHz of additional broadening in our microfabricated vapor cell. Assuming the entire additional broadening comes from collisional broadening [36] yields a background gas limit of less than 0.4 Torr (0.5 hPa). Sub-Doppler spectroscopy using the $^1S_0 \rightarrow {}^3P_1$ transition in Sr at 689 nm with a narrow linewidth of $2\pi \times 7$kHz would allow for a more sensitive measurement of collisional broadening and corresponding collision shifts [37] in these vapor cells and is the subject of future investigations.

To characterize the operational lifetime of these cells, we measure the normalized light transmission through the cell off resonance from the atomic transition while holding it above 300 °C for a period of several days. Several cells were evaluated with different glass compositions and surface coatings to gain an understanding of the role materials play in determining the lifetime. It is known that alkaline earth atoms diffuse into most glasses at sufficiently high temperatures [38], and darkening of the glass limits the operational lifetime of typical alkaline earth vapor cells [18,19].

Figure 4 shows results of these measurements for cells fabricated with and without an Al_2O_3 coating on aluminosilicate and borosilicate glass windows. To compare the aging behavior between different cells, we normalize the relative transmission of each cell to 100 % at a time equal to zero. We attribute the slow rise in relative transmission of the coated cells to more than 100 % to the changing transmission of etalons present in the absorption arm, as the oven temperature comes to equilibrium. The empty triangles show that the uncoated borosilicate cells held at temperatures of 300 °C (corresponding to an atomic absorption of 10 % to 20 %) begin to show signs of degradation within a day. The oven temperature was increased at about 60 h to reach an atomic absorption of 50 %, which resulted in much quicker aging of the cell, as shown by the rapid decrease in off resonance transmission. A separate borosilicate glass cell with 20 nm of Al_2O_3 coating (filled triangles) was operated at a temperature equating to 45 % atomic absorption and shows lifetimes of hundreds of hours with no signs of degradation. The aluminosilicate cells, shown by the square markers in Fig. 4, display similar aging characteristics to the borosilicate glass cells. For both types of glass, the coating of Al_2O_3 greatly extends the lifetime of the cell, demonstrating the effectiveness of the Al_2O_3 protection layer.

The coated BSG cell corresponding to the data shown in Fig. 4 has been tested without failure beyond 380 h at operating temperatures corresponding to Doppler-broadened absorption of 25 % to 30 % with more than 25 cycles of heating to operating temperature and returning to 25 °C (not shown). The cell lifetime measurements depicted in Fig. 4 represent temperatures ranging from about 300 °C to 350 °C, depending on the depth of absorption. Following these measurements, the same coated BSG and coated ASG cells were operated at hotter temperatures of around 450 °C, corresponding to Doppler-broadened absorption of more than 99 %, resulting in the cells becoming opaque more quickly, with the vast majority lasting no more than 50 h.

In conclusion, we demonstrate a microfabricated strontium atomic vapor cell that contains low background pressure contamination and operational lifetimes in excess of hundreds of hours. The manufacturing processes, DRIE of silicon, ALD of Al_2O_3 on glass, and anodic bonding, are all available using commercial deposition and bonding systems [29,30,39] and support wafer-level fabrication. Absorption spectroscopy of strontium at $\lambda = 461$ nm demonstrates the presence of strontium vapor within the cell. A measurement of the power-broadened linewidth reveals low background gas contamination. Lastly, depending on the glass type and operating temperatures, these

cells exhibit lifetimes in the hundreds of hours with dozens of heating and cooling cycles. Further investigations into extending the lifetimes of these cells include annealing the sapphire deposited on ASGs to form a polycrystalline layer [40] or, alternatively, increasing the thickness of the Al_2O_3 deposition layer on the silicon preform. The performance demonstrated here is already sufficient for stabilization of a 461-nm laser for use in laser cooling of Sr. Based on the increasing use and research of alkaline earth metals, there is great promise and application for these miniature vapor cells to be widely adopted.

In the future, we plan to investigate sub-Doppler spectroscopy in the microfabricated vapor cells using the narrow linewidth (7.4-kHz) transition at 689 nm. This spectroscopy will be a more sensitive probe of additional broadening mechanisms in the vapor cells and a laser stabilized to this transition could serve as an excellent optical frequency reference [25]. Detection of excitation of the 689-nm transition can be performed through shelving spectroscopy [25] using a 461-nm probe beam, with an optimal signal-to-noise ratio achieved with probe beam absorption levels near 50 % at 461 nm. The operational temperatures of the microfabricated vapor cells demonstrated here already support this requirement. As a result of the small vapor cell size, one can consider constructing smaller, compact ovens for portable applications. Assuming a purely radiative heating process of an object with surface area 5 cm^2 and an emissivity of 0.6 (i.e., ceramics), the power radiated at 300 °C is 1.8 W. Furthermore, there is the possibility of using laser ablation as an alternative method for generating strontium vapor and drastically reducing the volume of the entire apparatus to the size of the vapor cell, 0.63 cm^3 [27]. Additionally, the alkaline earth vapor cell microfabrication processes could be adapted toward the development of a compact atomic beam for precision spectroscopy [41], consisting of a high-temperature oven region and a low-temperature probe region, with improved optical access for fluorescence detection.

Funding. National Institute of Standards and Technology.

Acknowledgments. We thank Susan Schima for her help in the process of fabricating the atomic vapor cells. We thank Yang Li and Tobias Bothwell for their careful reading of and suggestions for the manuscript.The authors have filed a patent on this work (US Provisional Patent Application No. 63/268,922).

Disclosures. JMP: University of Colorado Boulder and NIST (P), JK: NIST (P), MTH: NIST (P).

Data availability. Data underlying the results presented in this paper are not publicly available at this time but may be obtained from the authors upon reasonable request.

REFERENCES

1. A. Horsley and P. Treutlein, Appl. Phys. Lett. **108**, 211102 (2016).
2. M. T. Simons, A. H. Haddab, J. A. Gordon, and C. L. Holloway, Appl. Phys. Lett. **114**, 114101 (2019).
3. H. Q. Fan, S. Kumar, R. Daschner, H. Kübler, and J. P. Shaffer, Opt. Lett. **39**, 3030 (2014).
4. T. H. Sander, J. Preusser, R. Mhaskar, J. Kitching, L. Trahms, and S. Knappe, Biomed. Opt. Express **3**, 981 (2012).
5. J. C. Fang and J. Qin, Sensors **12**, 6331 (2012).
6. M. Bulatowicz and M. Larsen, in *Proceedings of the Institute of Navigation Pacific Positioning, Navigation and Timing Meeting, Pacific PNT 2013-April*, p. 610 (2013).
7. A. Nikulin and T. S. de Smet, The Leading Edge **38**, 447 (2019).
8. G. A. Veloski, R. G. Hammack, J. I. Sams, L. D. Wylie, and K. Heirendt, in *Proceedings of the Symposium on the Application of Geophyics to Engineering and Environmental Problems, SAGEEP 2018-March*, p. 202 (2018).
9. S. K. Lee, K. L. Sauer, S. J. Seltzer, O. Alem, and M. V. Romalis, Appl. Phys. Lett. **89**, 214106 (2006).
10. S. Knappe, V. Shah, P. D. Schwindt, L. Hollberg, J. Kitching, L. A. Liew, and J. Moreland, Appl. Phys. Lett. **85**, 1460 (2004).
11. V. Maurice, Z. L. Newman, S. Dickerson, M. Rivers, J. Hsiao, P. Greene, M. Mescher, J. Kitching, M. T. Hummon, and C. Johnson, Opt. Express **28**, 24708 (2020).
12. K. Döringshoff, F. B. Gutsch, V. Schkolnik, C. Kürbis, M. Oswald, B. Pröbster, E. V. Kovalchuk, A. Bawamia, R. Smol, T. Schuldt, M. Lezius, R. Holzwarth, A. Wicht, C. Braxmaier, M. Krutzik, and A. Peters, Phys. Rev. Appl. **11**, 054068 (2019).
13. F. B. Dunning, T. C. Killian, S. Yoshida, and J. Burgdörfer, J. Phys. B: At., Mol. Opt. Phys. **49**, 112003 (2016).
14. J. L. Hall, M. Zhu, and P. Buch, J. Opt. Soc. Am. B **6**, 2194 (1989).
15. G.-W. Truong, D. Stuart, J. D. Anstie, E. F. May, T. M. Stace, and A. N. Luiten, Metrologia **52**, S324 (2015).
16. N. Lemke, K. W. Martin, J. Jackson, C. Erickson, J. Armstrong, and D. Durfee, in *2017 Joint Conference of the European Frequency and Time Forum and IEEE International Frequency Control Symposium* (IEEE, 2017), pp. 460–461.
17. A. Jayakumar, B. Plotkin-Swing, A. O. Jamison, and S. Gupta, Rev. Sci. Instrum. **86**, 073115 (2015).
18. J. L. Armstrong, N. D. Lemke, K. W. Martin, and C. J. Erickson, Slow Light, Fast Light, and Opto-Atomic Precision Metrology IX **9763**, 976303 (2016).
19. J. A. Neuman, P. Wang, and A. Gallagher, Rev. Sci. Instrum. **66**, 3021 (1995).
20. C. J. Erickson, B. Neyenhuis, and D. S. Durfee, Rev. Sci. Instrum. **76**, 123110 (2005).
21. Y. Li, T. Ido, T. Eichler, and H. Katori, Appl. Phys. B **78**, 315 (2004).
22. V. O. Lorenz, X. Dai, H. Green, T. R. Asnicar, and S. T. Cundiff, Rev. Sci. Instrum. **79**, 123104 (2008).
23. Y. Shimada, Y. Chida, N. Ohtsubo, T. Aoki, M. Takeuchi, T. Kuga, and Y. Torii, Rev. Sci. Instrum. **84**, 063101 (2013).
24. J. J. McFerran, J. G. Hartnett, and A. N. Luiten, Appl. Phys. Lett. **95**, 031103 (2009).
25. I. Manai, A. Molineri, C. Fréjaville, C. Duval, P. Bataille, R. Journet, F. Wiotte, B. Laburthe-Tolra, E. Maréchal, M. Cheneau, and M. Robert-De-Saint-Vincent, J. Phys. B: At., Mol. Opt. Phys. **53**, 085005 (2020).
26. N. Sekiguchi, T. Sato, K. Ishikawa, and A. Hatakeyama, Appl. Opt. **57**, 52 (2018).
27. O. Kock, W. He, D. Swierad, L. Smith, J. Hughes, K. Bongs, and Y. Singh, Sci. Rep. **6**, 37321 (2016).
28. M. Yasuda, T. Tanabe, T. Kobayashi, D. Akamatsu, T. Sato, and A. Hatakeyama, J. Phys. Soc. Jpn. **86**, 125001 (2017).
29. S. Woetzel, F. Talkenberg, T. Scholtes, R. Ijsselsteijn, V. Schultze, and H. G. Meyer, Surf. Coat. Technol. **221**, 158 (2013).
30. S. Karlen, J. Gobet, T. Overstolz, J. Haesler, and S. Lecomte, Opt. Express **25**, 2187 (2017).
31. J. A. Dziuban, *Bonding in Microsystem Technology* (Springer, 2006).
32. K. Jacob and Y. Waseda, J. Less-Common Met. **139**, 249 (1988).
33. M. Yasuda, T. Kishimoto, M. Takamoto, and H. Katori, Phys. Rev. A **73**, 011403 (2006).
34. S. B. Nagel, P. G. Mickelson, A. D. Saenz, Y. N. Martinez, Y. C. Chen, T. C. Killian, P. Pellegrini, and R. Côté, Phys. Rev. Lett. **94**, 083004 (2005).
35. U. Poschinger, W. Salzmann, N. Bouloufa, A. Crubellier, and O. Dulieu, Phys. Scr. **T134**, 014014 (2009).
36. Y. C. Chan and J. A. Gelbwachs, J. Phys. B: At., Mol. Opt. Phys. **25**, 3601 (1992).
37. N. Shiga, Y. Li, H. Ito, S. Nagano, T. Ido, K. Bielska, R. S. Trawiåski, and R. CiuryÅo, Phys. Rev. A **80**, 030501 (2009).
38. H. Mehrer, A. W. Imre, and E. Tanguep-Nijokep, J. Phys.: Conf. Ser. **106**, 012001 (2008).
39. D. G. Bopp, V. M. Maurice, and J. E. Kitching, JPhys Photonics **3**, 015002 (2021).
40. M. Broas, O. Kanninen, V. Vuorinen, M. Tilli, and M. Paulasto-Kröckel, ACS Omega **2**, 3390 (2017).
41. C. Li, X. Chai, B. Wei, J. Yang, A. Daruwalla, F. Ayazi, and C. Raman, Nat. Commun. **10**, 1831 (2019).